



HAL
open science

Charge-solvated versus protonated salt forms of cyclodepsipeptide toxins in electrospray: Dissociation of alkali-cationized forms enables straightforward sequencing of cereulide

Sophie Liuu, Kam Eng Trinh, Ekaterina Darii, Chenqin Cao, Annelaure Damont, Yves Gimbert, François Fenaille, Yassine Makni, Chanthadary Inthavong, Gwenaëlle Lavison-Bompard, et al.

► To cite this version:

Sophie Liuu, Kam Eng Trinh, Ekaterina Darii, Chenqin Cao, Annelaure Damont, et al.. Charge-solvated versus protonated salt forms of cyclodepsipeptide toxins in electrospray: Dissociation of alkali-cationized forms enables straightforward sequencing of cereulide. *Journal of Mass Spectrometry*, 2024, 59 (6), pp.e5037. 10.1002/jms.5037. hal-04578801

HAL Id: hal-04578801

<https://hal.science/hal-04578801v1>

Submitted on 17 May 2024







HAL is a multi-disciplinary open access archive for the deposit and dissemination of scientific research documents, whether they are published or not. The documents may come from teaching and research institutions in France or abroad, or from public or private research centers.

L'archive ouverte pluridisciplinaire **HAL**, est destinée au dépôt et à la diffusion de documents scientifiques de niveau recherche, publiés ou non, émanant des établissements d'enseignement et de recherche français ou étrangers, des laboratoires publics ou privés.



Distributed under a Creative Commons Attribution 4.0 International License

Charge-solvated versus protonated salt forms of cyclodepsipeptide toxins in electrospray: Dissociation of alkali-cationized forms enables straightforward sequencing of cereulide

Sophie Liuu¹  | Kam eng Trinh² | Ekaterina Darii³  | Chenqin Cao⁴ |
Annelaure Damont⁴ | Yves Gimbert^{5,6}  | François Fenaille⁴  | Yassine Makni² |
Chanthadary Inthavong² | Gwenaëlle Lavison-Bompard²  |
Jacques-Antoine Hennekinne¹ | Olivier Firmesse¹  | Jean-Claude Tabet^{4,5}

¹Staphylococcus, Bacillus & Clostridium (SBCL) unit, Laboratory for Food Safety, French Agency for Food, Environmental and Occupational Health & Safety (ANSES), Université Paris-Est, Maisons-Alfort, France

²Pesticides and Marine Biotoxins (PBM) unit, Laboratory for Food Safety, French Agency for Food, Environmental and Occupational Health & Safety (ANSES), Université Paris-Est, Maisons-Alfort, France

³Génomique Métabolique, Genoscope, Institut François Jacob, CEA, CNRS, Univ Evry, Université Paris-Saclay, Evry, France

⁴Université Paris Saclay, CEA-INRAE, Laboratoire Innovations en Spectrométrie de Masse pour la Santé (LI-MS), DRF/Institut Joliot/DMTS/SPI, MetaboHUB, CEA Saclay, Gif-sur-Yvette, France

⁵Faculté des Sciences et de l'Ingénierie, Institut Parisien de Chimie Moléculaire (IPCM), Sorbonne Université, Paris, France

⁶Département de Chimie Moléculaire, UMR CNRS 5250, Université Grenoble Alpes, Grenoble, France

Correspondence

Sophie Liuu, *Staphylococcus, Bacillus & Clostridium* (SBCL) unit, Laboratory for Food Safety, French Agency for Food, Environmental and Occupational Health & Safety (ANSES), Université Paris-Est, Maisons-Alfort, France.
Email: sophie.liuu@anses.fr

Funding information

Agence Nationale de la Recherche, Grant/Award Numbers: ANR-20-CE29-0017, ANR-19-CE21-0002, ANR-11-INBS-0010

Abstract

Bacillus cereus is responsible for foodborne outbreaks worldwide. Among the produced toxins, cereulide induces nausea and vomiting after 30 min to 6 h following the consumption of contaminated foods. Cereulide, a cyclodepsipeptide, is an ionophore selective to K^+ in solution. In electrospray, the selectivity is reduced as $[M + Li]^+$, $[M + Na]^+$ and $[M + NH_4]^+$ can also be detected without adding corresponding salts. Two forms are possible for alkali-cationized ions: *charge-solvated* (CS) that exclusively dissociates by releasing a bare alkali ion and *protonated salt* (PS), yielding alkali product ions by covalent bond cleavages (CBC) promoted by mobile proton. Based on a modified peptide cleavage nomenclature, the PS product ion series (**b**, **a**, $[b + H_2O]$ and $[b + C_nH_{2n}O]$ [$n = 4, 5$]) are produced by $Na^+/Li^+/K^+$ -cationized cereulide species that specifically open at ester linkages followed by proton mobilization promoting competitive ester CBC as evidenced under resonant collision activation. What is more, unlike the sodiated or lithiated cereulide, which regenerates little or no alkali cation, the potassiated forms lead to an abundant K^+ regeneration. This occurs by splitting of (i) the potassiated CS forms with an appearance threshold close to that of the PS first fragment ion generation and (ii) eight to

This is an open access article under the terms of the [Creative Commons Attribution](https://creativecommons.org/licenses/by/4.0/) License, which permits use, distribution and reproduction in any medium, provided the original work is properly cited.

© 2024 The Authors. *Journal of Mass Spectrometry* published by John Wiley & Sons Ltd.

four potassium residue product ions from the PS forms. Since from Na⁺/Li⁺-cationized cereulide, (i) the negligible Na⁺/Li⁺ regeneration results in a higher sensibility than that of potassium forms that abundantly releasing K⁺, and (ii) a better sequence recovering, the use of Na⁺ (or Li⁺) should be more pertinent to sequence isocereulides and other cyclodepsipeptides.

KEYWORDS

alkali, cereulide, cyclodepsipeptide, dissociation, electrospray

1 | INTRODUCTION

Bacillus cereus, a ubiquitous soil bacterium, is the first most frequently found causative agent in foodborne outbreaks (FBOs) in France¹ and the first cause of FBOs due to bacterial toxins in Europe.² The bacterium is responsible for two types of food-associated gastrointestinal diseases: a diarrheal syndrome, caused by enterotoxins produced in the gut, and an emetic syndrome, caused by preformed toxins. Symptoms are generally of short duration and evolve towards spontaneous recovery, but fatal cases have been reported.^{3–9} This study focused on one of these emetic toxins, cereulide (Figure 1). This toxin is a thermo-stable, 1.2 kDa dodecadepsipeptide with three repeated motifs [(D)A-(L)O_V-(L)V-(D)O_L]₃. Recently, a review was published on its characterization, impacts, and associated public precautions.¹⁰ It is a potassium ion-selective ionophore in solution. This property is attributed to the exact fitting of the K⁺ cation into the cavity created by the cyclic backbone of the dodecadepsipeptide in a hexagonal cylinder-like conformation¹¹ and stabilized by several lone pair electrons of heteroatoms as shown by NMR.^{11–13}

Mass spectrometry (MS) based on desorption processes is a particularly suitable tool for the analysis of cyclodepsipeptides. They were first studied using desorption techniques such as (i) fast atom bombardment (FAB) for analysis of cereulide¹¹ and (ii) matrix-assisted laser desorption ionization (MALDI) for fast and sensitive analysis of a colony smear of *Bacillus cereus* isolated from foods.^{14,15} Cyclodepsipeptide desorption by electrospray (ESI) in positive mode competitively yields protonated and sodiated species ([M + H]⁺ and [M + Na]⁺, respectively), depending on the desolvation voltage.¹⁶ Furthermore, the relative abundances of ammonium and potassium cereulide depend non-linearly on the salt amount added into the solution.¹⁷ This suggests a selectivity towards K⁺ compared to the sodiated species.¹⁷ More recently,¹³ the ESI mass spectrum of cereulide showed its cationized species by NH₄⁺, Na⁺, and K⁺ ions, present in trace amounts in the solution and/or source. All these studies show significant variability of the species desorbed in ESI, depending on the experimental conditions, which may hide the natural selectivity of cereulide for K⁺. Consequently, many precautions need to be taken to ensure good reproducibility of mass spectra in order to guarantee selectivity towards a particular cation and thus ensure the robustness of the associated analytical results. Nevertheless, identification and reliable quantification of cereulide are possible by ESI MS, as shown

by interlaboratory comparisons following the EN ISO18465 standard using ammonium adduct ion¹⁸ instead of the potassium cereulide species.^{13,15,19,20}

In the gas phase, small size alkali-cationized polyfunctional molecules (e.g., amino acids and peptides²¹) can be characterized by two possible competitive generic structures^{22,23}: (i) a *charge-solvated* or *cation-solvated* (CS) structure and/or (ii) a *protonated salt* (PS) structure, the typical form generated by electrospray^{24–27} and by MALDI.²⁷ In the CS form, the alkali cation is solvated by heteroatom electron-lone pairs of the molecule in its *canonical* form (i.e., without balanced apparent charges), yielding weak interactions with alkali. In contrast, in the PS form, the alkali interacts with the anionic site of a *zwitterion* form of the molecule, with a strong ion/ion interaction. Note that the structure of some alkali-cationized amino acids^{22,28–32} and peptides^{27,33,34} could be in *zwitterion* form in competition with their *canonical* form. The latter, resulting in CS form, is described for sodiated dipeptides and tripeptides (with G or A as residues) yielding exclusively Na⁺ release.³⁴ The PS structure, with ion/ion interaction, differs from a hydrogen-bonded (HB) form (two neutrals solvating proton, formally) of [M + NH₄]⁺ involving the M structure only in *canonical* form, although the latter leads to a mobile proton via the formation of [M + H]⁺. In PS, the mobile proton at the positive site of the *zwitterion* can competitively migrate to various sites, resulting in a mixture of protomers.^{24–26} The existence and distribution of the different CS and PS tautomer forms of cationized molecules (Text S1) depend on the aggregate desolvation voltage.^{35,36} This property specifically influences inter- and intramolecular interactions. In a recent review on dissociations of cationized amino-acids and small peptides, Armentrout²¹ investigated the CS/PS coexistence by mechanistic and energetic studies using threshold collision-induced dissociation (TCID) measurements of product ions with a homemade guided ion beam tandem mass spectrometer (GIBMS).

In the case of a collisionally activated PS form, the mobilized proton promotes covalent bond cleavages (CBC), resulting in the retention of the alkali cation either in the product ions or in the released neutral salts.³⁷ **b** series ions are exclusively cationized as (**b**_i-H + Na) for sodiated peptides with an acidic residue in the position *i*. The Na⁺ retention in product ions reflects the presence of salt.²⁷ This behavior contrasts with that of the CS forms that decompose exclusively by regeneration of the naked alkali cation.²⁵ This interpretation is an alternative to the proposed mechanisms based on charge remote

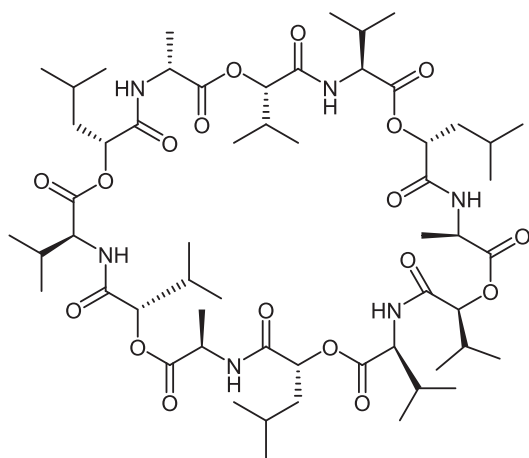


FIGURE 1 Structure of cereulide.

fragmentation-like from sodiated ionophore, as proposed by Crevelin et al.³⁸ and Demarque et al.,³⁹ where herein (i) the charge does not induce dissociations and (ii) the alkali is spectator to the dissociations.

As potassiated cereulide, $[M + K]^+$, is implicitly considered as a CS form,^{13,15,19,20,40} it should then decompose by regenerating the bare alkali K^+ cation under low-energy collision-induced dissociation (CID) conditions.^{25,37} This contrasts with the published CID spectra where K^+ detection is omitted due to the commonly used m/z range and where fragment ions are shifted by $+38 m/z$ relative to those from the $[M + H]^+$ dissociations.^{13,19,20} This suggests K^+ retention in fragment ions, resulting from CBC processes. Marxen et al.¹³ consider that these ions are formed first by the hydrolysis of ester bonds, followed by consecutive CBC processes. This implies that the cationized cereulide in a CS structure cannot be the source of these product ions. In other words, how could the alkali cation lead, through “hydrolysis”, to the opening of the CS form of cereulide?

In order to lift the veil on CS versus PS ambiguity^{26,37} regarding $K^+/Na^+/Li^+$ -cationized cereulide structures, energy-resolved mass spectrometry (ERMS) breakdown curves^{41–43} based on non-resonant collisional activation²⁵ of the selected alkali-cationized cereulide were explored using different high resolution tandem instruments. In particular, the total ion current in absolute values of the set of product ions related to the ERMS of each of the lithiated, sodiated, and potassiated cereulide species was compared to that related to the ERMS of the ammonium adduct ion to estimate the extent of the bare alkali cation discrimination resulting from their scattering at the highest collision energies (E_{Lab}). The scattering effect at the highest E_{Lab} is all the more pronounced as the m/z is low^{44,45} (Lesage et al, to be published). To our knowledge, such an approach to evaluate the effect of scattering on the detection of Li^+ , Na^+ , and K^+ has never been performed using commercial instruments.^{46,47} This study documents (i) the driving force leading to the CBC responsible for the formation of the most representative product ions of the cereulide sequences, (ii) the double origin of K^+ release, and (iii) the choice of the alkali-cationized cereulide to sequence the cereulide with the highest sensitivity.

2 | METHODS

2.1 | Chemicals and reagents

Standard synthetic cereulide was produced by Chiralix (Nijmegen, the Netherlands). Cereulide standard was dissolved in methanol purchased from Fisher Scientific (Illkirch-Graffenstaden, France). Potassium chloride (KCl) and lithium chloride (LiCl) were purchased from Merck (Darmstadt, Germany).

2.2 | Mass spectrometry

All the experiments were performed using various tandem instruments based on high resolution analyzers, such as Time-of-Flight: (i) *TripleTOF 5600* (ABSciex, Darmstadt, Germany) and (ii) *Impact HD* (Bruker Daltonics, Bremen, Germany), and very high-resolution Fourier transform analyzers, such as Orbitrap: (i) *Q Exactive* (Thermo Scientific, Bremen, Germany) and (ii) *Orbitrap Elite* (Thermo Scientific, Courtaboeuf, France). Alkali-cationized cereulide species were produced under ionization/desorption by ESI in positive mode using direct ion injection through a syringe pump. For Qq/TOF *Impact HD* instrument, KCl and LiCl were added for enhancing the corresponding alkali-cationized cereulide, and two calibrations of the m/z scale were used (Table S1). The first one, applied by default, does not allow the detection of alkali cations, while the second one enables detection of all but not lithium. Optimization of sodium detection was achieved using sodiated PEG10, which exclusively released neutral PEG and the naked Na^+ ion without significant TIC decrease.²⁵ However, this optimization suffers from discrimination in the ion detection from m/z 200 to m/z 100. For this reason, the product ion spectra of these alkali-cationized molecules were also recorded using the default calibration mode. MS/MS experiments were performed under non-resonant ion activation conditions with both the Qq/TOF instruments, as well as in the HCD cell of both the Qq/Orbitrap and LIT/Orbitrap instruments. Resonant ion excitation for sequential MS^n experiments was performed in the ion trap cell using the LIT/Orbitrap mass spectrometer. To simplify the experimental part of this article, all details on the optimized experimental conditions are reported in Table S1. The ERMS breakdown curves from non-resonant excitation experiments were constructed using the relative abundance values of the precursor and product ions. To show some bias from the relative abundance use, absolute values of the abundance of these ions were also used for building the ERMS breakdown curves.

2.3 | Annotations and nomenclature

1. The *total ion current* (TIC), based on the absolute ion abundances, is used to show the scattering effect resulting in the partial loss of the low m/z product ions occurring at the highest collision energies.

- The *total product ion current* (TPIC) corresponds to the sum of abundances of all the product ions. This simplifies in one profile, the set of product ion profiles that constitute the ERMS breakdown curves when many product ions are generated by CBC (i.e., for the PS form). This TPIC allows for better comparison with TIC to highlight, at the highest collision energies, the loss of product ions with low m/z ratios. TPIC* is used when the alkali cation abundance was removed from TPIC.
- The *precursor ion current* (PIC) corresponds to the abundance of the survivor precursor ion.
- Collisional spectra*: the nomenclature used for product ion spectra is consistent with IUPAC recommendations.⁴⁸ However, IUPAC recommends CID as a generic name for collisional excitation, regardless of whether resonant or non-resonant excitation mode is used. One commercial company has called the former CID and the latter HCD (higher collision energy),⁴⁹ which may confuse the nomenclature based on that recommended by IUPAC, especially when tandem from other companies is used. This is why we have used “resonant” and “non-resonant” here.
- Collision energy* (E_{Lab}): the eV unit is used as collision energy for the Qq/TOF-based tandem instruments. For Orbitrap-based tandem instrument, the normalized collision energy (NCE)⁵⁰ in % is used (Figures S3–S5). For various singular points of the different ion profiles, a collision energy is defined as (i) the energy threshold for the appearance of m/z product ions ($E_{\text{Lab,Thre},m/z}$) and for TPIC* ($E_{\text{Lab,Thre},\text{TPIC}^*}$), (ii) the collision energy to reach the apex for a particular monomodal profile of a product ion ($E_{\text{Lab,apex},m/z}$) or for TPIC* ($E_{\text{Lab,apex},\text{TPIC}^*}$), and (iii) the collision energy at the half-height of the negative sigmoid for the survivor precursor ion ($E_{\text{Lab},1/2,\text{PIC}}$) or positive sigmoid for the latest-generation m/z product ions ($E_{\text{Lab},1/2,m/z}$) or for TPIC* ($E_{\text{Lab},1/2,\text{TPIC}^*}$). These characteristic collision energies must be converted in collision energies at the center of mass ($E_{\text{COM}} = E_{\text{Lab}}[m_{\text{T}}/(M + m_{\text{T}})]$, m_{T} = the gaseous target mass as N_2) to be compared to the characteristic energies involving other alkali cations or other values for same system (or considered as similar) provided from literature.
- Residue annotation*: the amino acid residues are annotated by the one-letter code (alanine, A; valine, V; leucine, L). The α hydroxy alkyl acid residues as the 2-hydroxy-3-methyl-butanoic acid or 2-hydroxyisovaleric acid ($\text{C}_5\text{H}_8\text{O}_2$) and the 2-hydroxy-4-methyl-pentanoic acid or 2-Hydroxyisocaproic acid ($\text{C}_6\text{H}_{10}\text{O}_2$) are annotated by one-letter code based on the amino acid residue code considering that the amino group substituted by one hydroxyl group is written as an O letter in superscript such as $^{\text{O}}\text{V}$ and $^{\text{O}}\text{L}$, respectively. Concerning the chirality annotation, *dexter* (D) and *laevus* (L) are written in superscript and in parentheses such as $^{(\text{D})}\text{A}$, $^{(\text{L})}\text{V}$, $^{(\text{L})}\text{O}\text{V}$, and $^{(\text{D})}\text{O}\text{L}$. Peptide cleavage nomenclature is detailed in Text S2.

3 | RESULTS AND DISCUSSION

Under the chosen ESI source conditions of the high resolution Qq/Orbitrap instrument (Q *Exactive*, Thermo Scientific), the mass

spectrum of cereulide in methanol presents the adduct $[\text{M} + \text{NH}_4]^+$ (m/z 1170, 38% of base peak), $[\text{M} + \text{Li}]^+$ (m/z 1159, 4% of base peak), $[\text{M} + \text{Na}]^+$ (m/z 1175, as base peak), and $[\text{M} + \text{K}]^+$ (m/z 1191, 25% of base peak) ions (Figure S1). This adduct ion distribution differs from what has been described in previous studies.^{13–17,40} These differences were expected since the source and instrument parameters affect the distribution of the desorbed molecular species (adduct ion or not) as well as the aggregate desolvation conditions in the reduced pressure zone.^{51–53}

Tandem MS experiments (MS^2), under low energy collisional conditions, were performed using various instruments to explore respective cereulide ion structures (intact cyclic vs opened ring forms) and consequently, to elucidate the origin of their respective product ions (Figure 2).

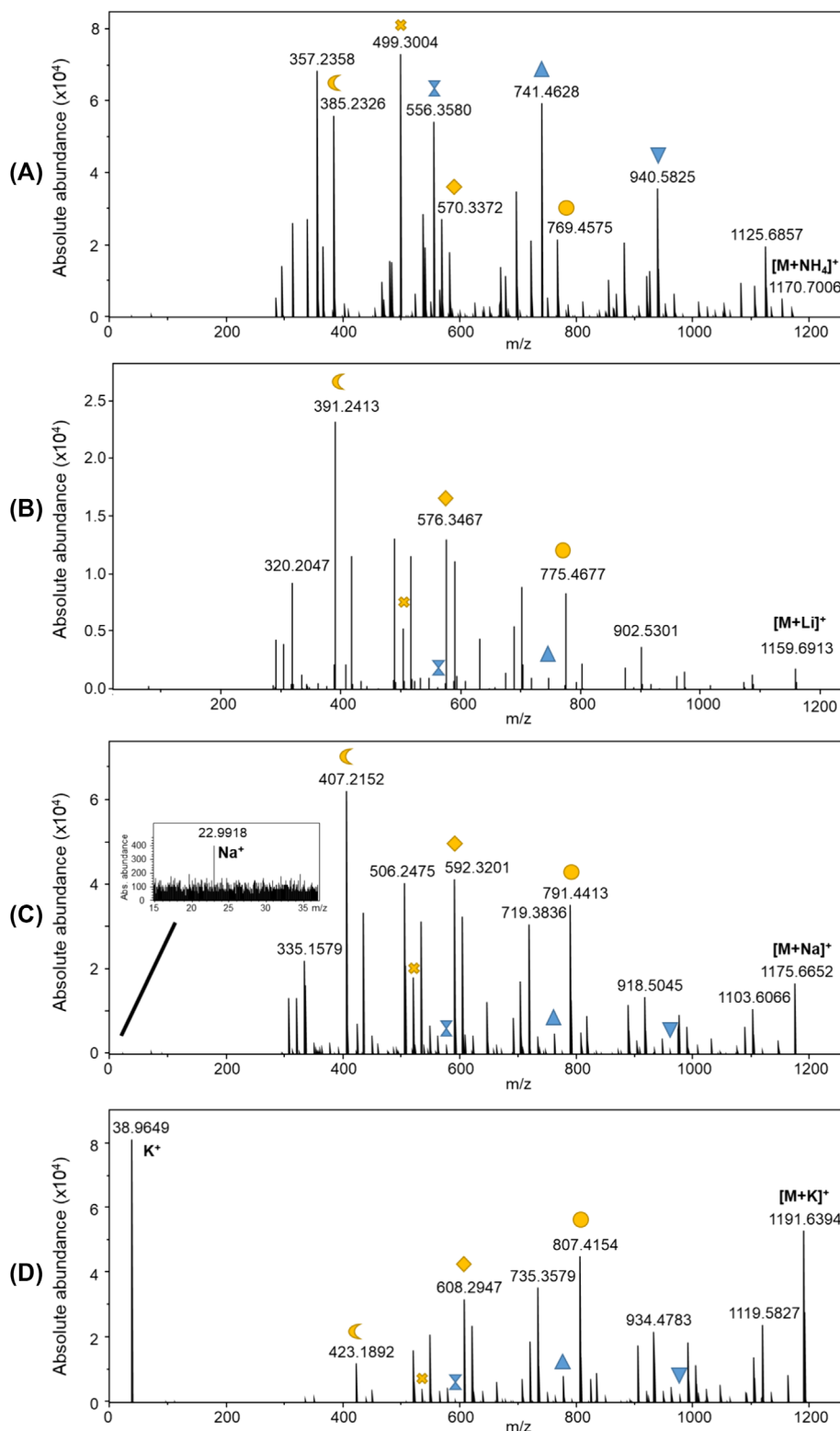
Qq/TOF instruments (*Impact HD* and *TripleTOF 5600*) were used to detect alkali cations (Figure 2). Product ions generated from these instruments are reported in Table S2. The product ions displayed in the collisional spectra (Figure 2B–D) of $[\text{M} + \text{Li}]^+$, $[\text{M} + \text{Na}]^+$, and $[\text{M} + \text{K}]^+$ are mainly characterized by m/z values shifted by +6.01, +21.98, and +37.96 m/z , respectively, compared to those of product ions of the second generation (through the formation of $[\text{M} + \text{H}]^+$ ions) from the dissociation of $[\text{M} + \text{NH}_4]^+$. These results demonstrate that alkali cations are retained on the fragment ions produced by CID of alkali-cationized cereulide. Finally, the $[\text{M} + \text{K}]^+$ ion dissociation significantly regenerated the bare K^+ cation in contrast with lithiated and sodiated cereulide, which does not release Li^+ and no abundant Na^+ ions (less than 1% of base peak) under the non-resonant excitation conditions used (i.e., a common value used as $E_{\text{Lab}} = 94$ eV; Figure 2). The detection of these alkali cations from alkali-cationized cereulide has never been reported in previous studies since their presence is often overlooked.^{13,15,19,20,40} Yet their possible detection should be of great help to describe the CS/PS structure(s) of alkali-cationized cereulide.

3.1 | Coexistence of the CS and PS forms of alkali-cationized cereulide

In order to determine the relative proportion of CS and PS forms characterizing the alkali-cationized cereulide species according to the alkali cation, their ERMS breakdown curves were studied. Recorded with a particular instrument tuning and calibration allowing alkali detection using Qq/TOF instrument, ERMS breakdown curves of the $[\text{M} + \text{NH}_4]^+$ (m/z 1170), $[\text{M} + \text{Li}]^+$ (m/z 1159), $[\text{M} + \text{Na}]^+$ (m/z 1175), and $[\text{M} + \text{K}]^+$ (m/z 1191) were compared. Especially, (i) their relative abundances (Figure 3) and (ii) their absolute abundances⁴⁶ (Figure 4) were explored. The main characteristics of the PIC, TPIC, or TPIC* and alkali cation profiles from ERMS with relative abundance (Figure 3) are reported in Table S3.

Instead of the default calibration (Figure S2) where alkali cation detection is systematically missed, the choice to use low m/z calibration (Figures 3 and 4) was motivated by the need to compare the

FIGURE 2 Product ion spectra of (A) $[M + \text{NH}_4]^+$, m/z 1170 ($E_{\text{Lab}} = 60$ eV); (B) $[M + \text{Li}]^+$, m/z 1159 ($E_{\text{Lab}} = 94$ eV); (C) $[M + \text{Na}]^+$, m/z 1175 ($E_{\text{Lab}} = 94$ eV); and (D) $[M + \text{K}]^+$, m/z 1191 ($E_{\text{Lab}} = 94$ eV). Each of the product ion series is annotated with a common label color in (B)–(D), respectively, shifted by +6.01, +21.98, and +37.96 m/z from those assigned to the same series displayed in (A). The m/z scale calibration was adapted to detect the K^+ and Na^+ ions and not for that of Li^+ using a Qq/TOF instrument (*Impact HD*, Bruker).



breakdown profiles of the different product ions at low m/z ratios, for example, m/z 72 and m/z 44 from the ammonium adduct ion (detected in low relative abundance for $[M + \text{Li}]^+$ and $[M + \text{Na}]^+$ and absent for $[M + \text{K}]^+$) and alkali m/z 23 and m/z 39 ions for $[M + \text{Na}]^+$ and for $[M + \text{K}]^+$, respectively. Alkali cations are released from $[M + \text{Na}]^+$ at the highest collision energies, but from $[M + \text{K}]^+$ at the

lowest. The abundance decrease at the highest energies is due to enhancement of the low m/z product ion scattering (Figure 4), as described in a recent study.⁴⁶ To simplify the study of these breakdown profiles, each of the alkali cation profiles was compared to a profile resulting from the absolute abundance sum of the other numerous product ions (i.e., TPIC*; Figure 4B–D). In addition to the

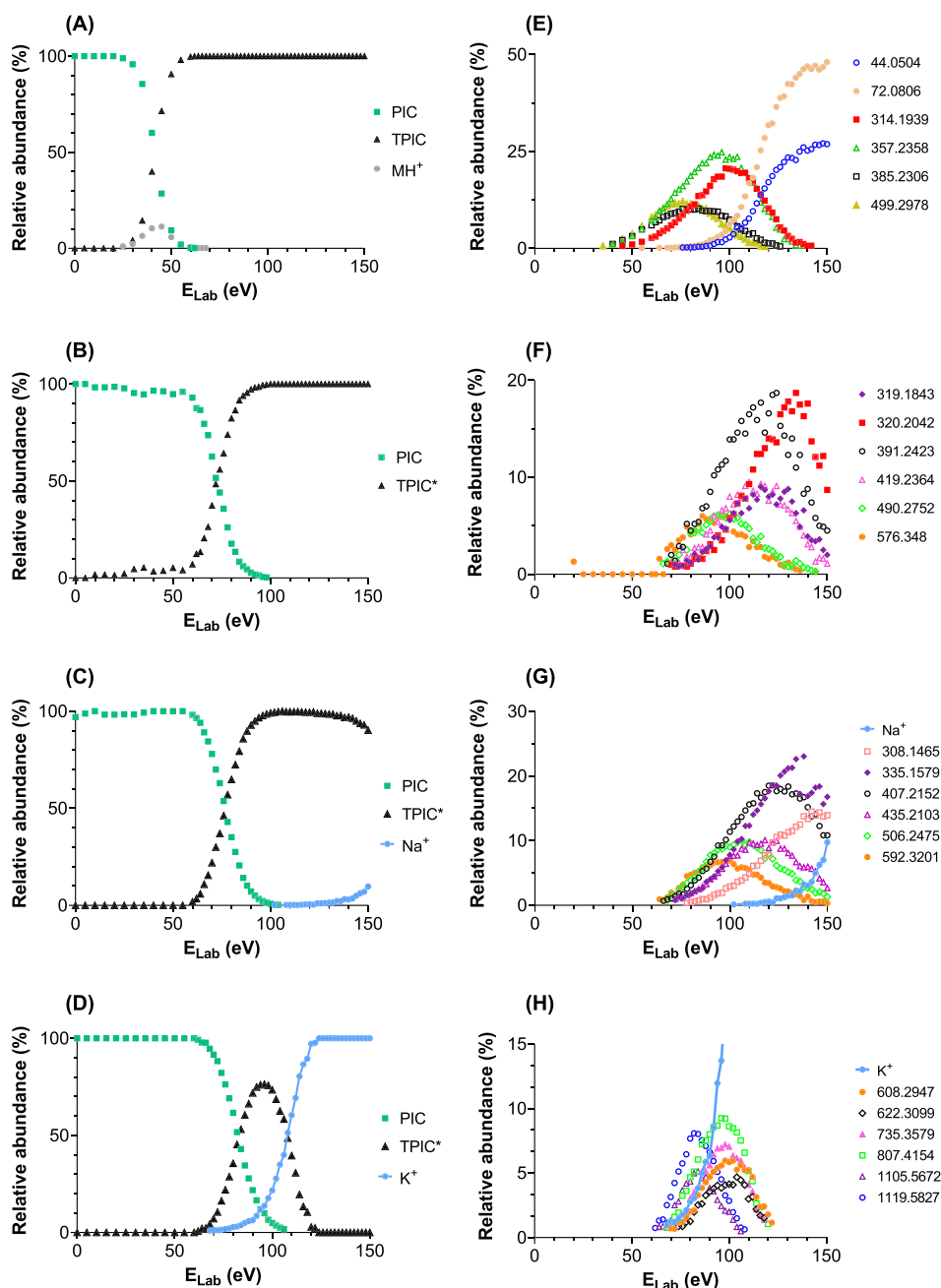


FIGURE 3 ERMS breakdown curves of the ammonium adduct and alkali-cationized cereulide ($0 \text{ eV} < E_{\text{Lab}} < 150 \text{ eV}$): (A, E) $[M + \text{NH}_4]^+$ (m/z 1170), (B, F) $[M + \text{Li}]^+$ (m/z 1159), (C, G) $[M + \text{Na}]^+$ (m/z 1175), and (D, H) $[M + \text{K}]^+$ (m/z 1191). In (A)–(D), the profiles are based on the relative abundances corresponding to (i) the PIC (■), (ii) the TPIC or TPIC* (▲), and (iii) the Na^+ and K^+ ions for cationized molecules (●). In (E) and (F), detailed profiles of the six main product ions are reported. At the highest E_{Lab} values, the lithiated and sodiated cereulide species also dissociate into the ammonium m/z values (m/z 44 and m/z 72 ions), non-reported being not enough abundant. In (G) and (H), detailed profiles of the seven main product ions, including Na^+ and K^+ , are reported. In (H), to detail the seven main fragment ion profiles, K^+ relative abundance was limited to 15%. Experiments were performed under non-resonant excitation conditions using Qq/TOF (*Impact HD*, Bruker), with the m/z scale calibration adapted for K^+ and Na^+ detection but not that of Li^+ .

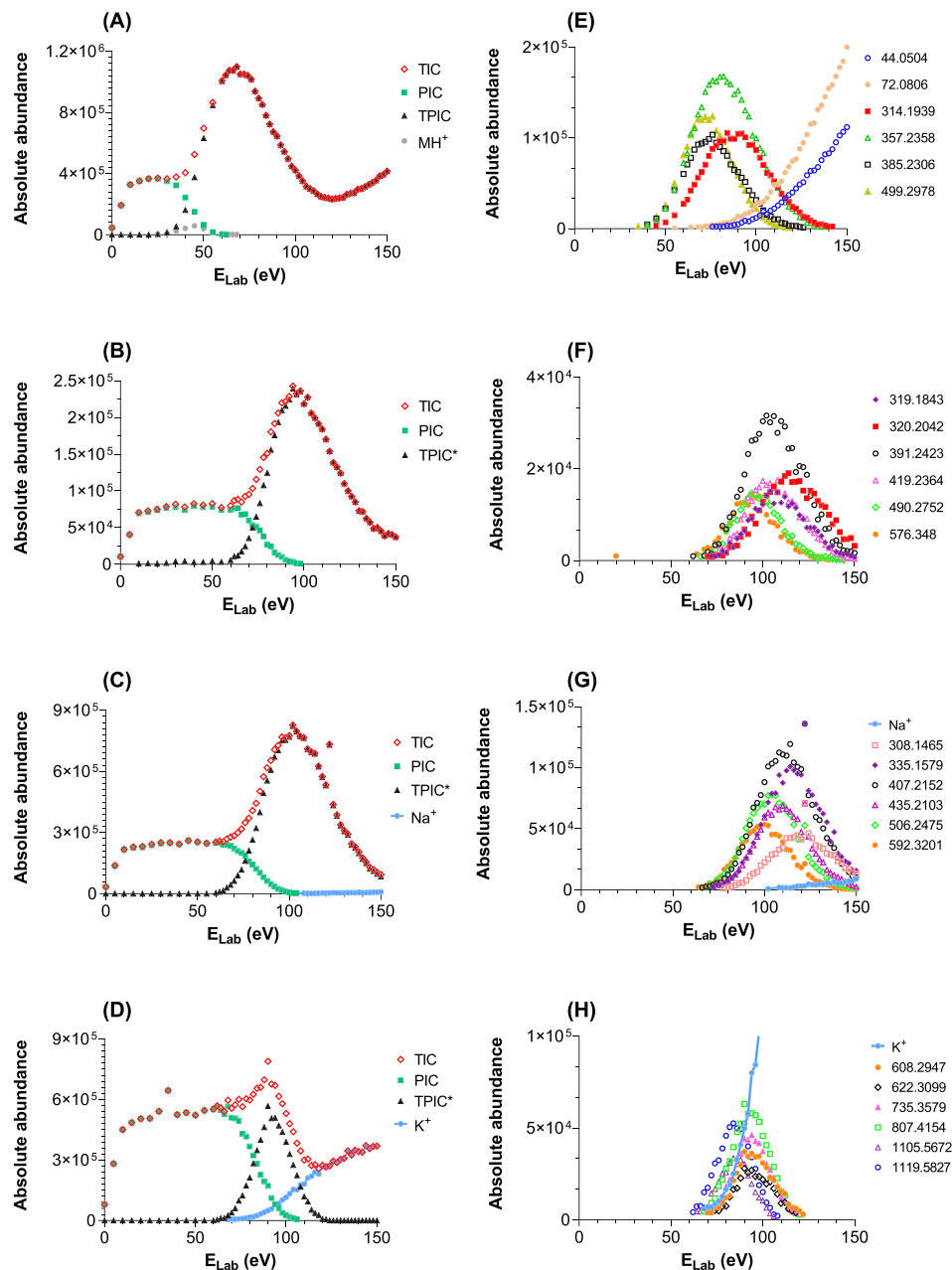
alkali cation, the six most abundant product ions are detailed in Figure 4F–H.

First, both K^+ and Na^+ cations were detected, but neither at the same energy threshold value ($E_{\text{Lab, Thre, 39}} = 64 \text{ eV}$ and $E_{\text{Lab, Thre, 23}} = 102 \text{ eV}$, respectively; Tables 1 and S3) nor at a similar abundance (Figures 3 and 4). Li^+ was not detected as it is below the detection m/z range. Second, alkali-cationized product ions are exclusively generated by CBC processes from the PS form in contrast to naked alkali cation regeneration, which can result from direct splitting of the CS form (detailed *vide infra*; Text S1). However, alkali cation regeneration cannot be excluded from PS forms if (i) a structural factor weakens the ion/ion interaction or/and (ii) the size of the alkali cation does not allow for a strong ion/ion interaction.

3.1.1 | Retention of the alkali cation in product ions from the sequential MS^3 experiments

Interestingly, during consecutive dissociations of selected cationized product ions from CID, alkali cation is retained as confirmed by collisional spectra using sequential MS^3 experiments performed in non-resonant mode using HCD cell of the *Orbitrap Elite* instrument (Figures S3 and S4). In fact, the cationized m/z 807 product ion (the main ion species related to the loss of the tetra-residue unit), formed from $[M + \text{K}]^+$ (m/z 1191), consecutively dissociates to give rise mainly to m/z 608 and m/z 423 (Figure S3C), with cation retention, as observed in the MS^2 experiment (Figure 2D). Their respective m/z ratios are roughly shifted by (i) -32 m/z to m/z 576 and m/z 391 from

FIGURE 4 ERMS breakdown curves of the ammonium adduct and the alkali-cationized cereulide ($0 \text{ eV} < E_{\text{Lab}} < 150 \text{ eV}$): (A, E) $[M + \text{NH}_4]^+$ (m/z 1170), (B, F) $[M + \text{Li}]^+$ (m/z 1159), (C, G) $[M + \text{Na}]^+$ (m/z 1175), and (D, H) $[M + \text{K}]^+$ (m/z 1191). In (A)–(D), the profiles are based on the absolute abundances which correspond to (i) the TIC (\diamond), (ii) the PIC (\blacksquare), (iii) the TPIC or TPIC* (\blacktriangle), and (iv) the Na^+ and K^+ abundances (\bullet). In (E)–(H), only detailed profiles of main product ions, including Na^+ and K^+ , are reported. In (H), to detail the main fragment ion profiles, the K^+ absolute abundance was limited to 1×10^5 a.u. Experiments were performed under non-resonant excitation conditions using Qq/TOF (*Impact HD*, Bruker), with the m/z scale calibration adapted for K^+ and Na^+ detection and not for that of Li^+ .



the product ion m/z 775 by consecutive dissociations of the lithiated cereulide (Figure S3A) and (ii) -16 m/z to m/z 592 and m/z 407 from dissociation of the selected sodiated product ion (m/z 791) (Figure S3b). These product ion pairs are also observed in the respective MS^2 collisional spectra (Figure 2B,C). In the same way, a similar trend characterizes the fragment m/z 1087, m/z 1103, and m/z 1119 ions generated from the small size 72 u loss from $[M + \text{Li}]^+$ (m/z 1159) (Figure S4A), $[M + \text{Na}]^+$ (m/z 1175) (Figure S4B), and $[M + \text{K}]^+$ (m/z 1191) (Figure S4C), respectively. All their respective product ions resulting in consecutive dissociations produce alkali retention (Figure S4) and correspond to the same losses of neutral residues as those from the cleavages of cationized cereulide (Figure 2).

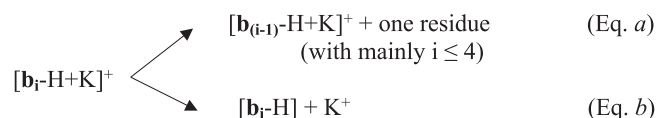
These experiments show that the structures of these selected product ions are in the PS form (consecutive decompositions by

CBCs) rather than in CS. In addition, for lithiated and sodiated selected product ions from these PS forms, the ion/ion interactions are stronger than the covalent bonds activated by a free neighbored positive charge related to the mobile proton.^{24–26} Consequently, this highlights the stability of interaction between the alkali and the negative charge of zwitterion (related to the opened ring form), which is preserved in the second-generation product ions with small neutral residues released (i.e., consisting of one or two residues; Figures S3 and S4). As small as two lithiated or sodiated residue product ions are detected, which is not the case for potassiated cereulide. Also, for the latter, abundance is reduced for product ions with less than eight residues with a minimum of four residues (Figures 2D, S3C, and S4C), which constitutes a product ion “cut-off.” This can suggest that the potassiated protonated salt splitting is possible.

3.1.2 | Possible double origin of the bare alkali cation depending on the alkali size and residue number in the product ions

Product ions above m/z 200 for $[M + Li]^+$ and $[M + Na]^+$ are similar in abundance but shifted by $+16 m/z$ (Table S2). However, a close examination at the abundance of the cationized tetra-peptide unit reveals that fragment ions above m/z 410 from the collision spectrum of $[M + Na]^+$ are slightly higher than those of analogous product ions from $[M + Li]^+$ under non-resonant conditions (Figure 2B,C; Table S2). In these conditions, this effect is most obvious for the analog fragment ions of $[M + K]^+$ (Figure 2D; Table S2). Moreover, it is also observed in sequential MS³ spectra of product ions in non-resonant mode (Figures S3 and S4). Parent ion appears to be more stable (relative abundance of $[M + Li-384]^+ < [M + Na-384]^+ < [M + K-384]^+$), which is a wrong interpretation as the abundance of MS³ product ions is reduced due to the release of bare alkali cation, not detected, which artificially increases the abundance of the parent ions (Figure S3). It is the same trend for $[M + Li/Na/K-72]^+$ parent ions (Figure S4). This variation in abundance is all the greater as the product ions are formed at the highest collision energies (i.e., via consecutive dissociations) and as the involved cation changes from Li⁺ to Na⁺ and from Na⁺ to K⁺ as confirmed by the evolution of TIC vs. E_{Lab} (Figure S5). In fact, the TIC values decrease to 10% of the TIC apex, beyond NCE = 40%, around NCE = 55% and NCE = 60% from dissociations of $[M + K-384]^+$, $[M + Na-384]^+$, and $[M + Li-384]^+$, respectively. Noteworthy and contrary to what is observed under the highest collision energy conditions for sodiated or lithiated cereulide, the formation of potassiated peptide fragment ions smaller than the cationized tetra-peptide unit species, resulting from consecutive dissociations, is hindered (Figures S3 and S4; Table S2). A similar trend characterizes dissociation of other potassiated cyclodepsipeptides compared to the corresponding lithiated and sodiated molecules, which is the case for instance of beauvericin,^{54,55} didemnin B,⁵⁴ enniatins,⁵⁴⁻⁵⁷ aplidine,⁵⁸ destruxins,⁵⁹ isariins,⁶⁰ isaridins,⁶⁰ and valinomycin.⁵⁷ This was first explained by the possibility to release the alkali cation from small size cationized product ion without more evidence.⁵⁷

Nevertheless, this idea needs to be clarified to better account for this behavior using our experimental results. This can be explained by considering the possible effect of the proximity of the protonated site on the salt bridge O⁻/K⁺ (vide infra) in potassiated fragment ions consisting of only two or three peptide residues (e.g., product ions as b₃ and b₂). This may weaken the ion/ion interaction or allow the transfer of the mobile proton to the alkoxide site, thereby enhancing alkali cation release in addition to the splitting of the CS form (Figures 2, S3, and S4; Table S2). In summary, these competitive reactions from the cationized b_i-product ion consist of (i) CBC of b_i to the b_(i-1) product ion (Eq. a) and (ii) regeneration of the alkali cation by splitting of the b_i product ion (Eq. b) as reported in the equations below:



This behavior might be explained by considering the orbital interactions according to Pearson's HSAB theory.⁶¹ Since K⁺ is more polarizable than the "hard acid" Na⁺, the former is better considered a "soft acid." The alkoxide group must be considered a hard base (see Text S4).⁶² As the orbital interactions between the "soft acid" and "hard base" may not be favorable, therefore, the ion/ion interaction will be significantly weaker than that occurring with "hard acid" (as Na⁺ or Li⁺). This model was also used by Banerjee et al.⁶⁰ to explain the difference of dissociation orientation of cationized isaridins according to the acidity hardness of cation (Li⁺ vs Na⁺ and Na⁺ vs K⁺ [and Ag⁺]).⁶⁰

Since the previous discussion shows that alkali cation regeneration can take place from splitting of small cationized product ions formed from cationized cereulide in PS form, its direct regeneration by "desolvation" of cationized cereulide in CS form is also possible. This direct process can be demonstrated by comparing the approximate threshold energy ($E_{Lab,Thre,m/z}$) of Na⁺ and K⁺ with those of

TABLE 1 Estimation of the cereulide/cation bond energy by energy threshold evaluation from alkali cation profiles extracted from ERMS of cationized cereulide using Qq/TOF instrument (calibrated for low m/z ion detection) and comparison with corresponding values with the 12-crown-4-ether measured by GIBMS.⁶³

	M = Cereulide/alkali interaction			M = 12-crown-4-ether ⁶³
	$E_{Lab,Thre}$ (eV)	E_{COM}^a (eV)	Bond energy (kJ/mol)	Bond energy in eV (kJ/mol)
$[M + K]^+$ (m/z 1191)	64	1.47	142	1.96 (189)
$[M + Na]^+$ (m/z 1175)	102	2.37	229	2.61 (252)
$[M + Li]^+$ (m/z 1159)	153 ^b	3.61 ^b	348 ^b	3.85 (371)

^aCalculated using the $E_{COM} = E_{Lab}[m_T/(M+m_T)]$ relation (m_T , the gaseous target mass as N₂) from the $E_{Lab,Thre}$ value estimated; this E_{COM} values considered as an energy maximum for the bare alkali regeneration.

^bThe measured bond energy increment (i.e., +1.24 eV) from the sodiated 12-crown-4-ether to the lithiated 12-crown-4-ether is used to the lithiated cereulide for estimating the $E_{Lab,Thre}$ to regenerate the bare Li⁺ ion.

cationized molecules with same alkali exclusively shown to be in CS form (Text S5). For this comparison, sodiated PEG10 was first chosen²⁵ using Qq/TOFMS, and for accurate binding, energy measurements were determined for sodiated and potassiated crown ethers using homemade GIBMS from Armentrout.⁶³ The accurate determinations are compared with those obtained from sodiated and potassiated cereulide species (Table 1).

To interpret the low abundance of the bare Na⁺ cation, characterized by a high energy appearance threshold ($E_{\text{Lab,Thre},23} = 102$ eV, i.e., $E_{\text{COM}} = 2.37$ eV roughly corresponding to an energy bond of 229 kJ/mol; Table 1) in comparison with sodiated crown-ether, it is necessary to ensure that the low mass discrimination is neglectable using the Qq/TOF instrument fine tuned for the low m/z ion detection. By considering that Li⁺ regeneration must be virtually absent in this range of collision energies used ($E_{\text{Lab,Thre},7}$ estimated as 153 eV; Table 1) and the K⁺ detection is possible with a weak discrimination ($E_{\text{Lab,Thre},39} = 64$ eV), a comparison of TIC profiles can provide decisive information. To compare these different TICs, each of them was normalized by its apex (reported in Figure S6). In this way, these TICs can be compared to estimate the influence of the low m/z ion discrimination on the detection of the bare Na⁺ ion according to the calibration used.

As the series of product ions from $[M + \text{Na}]^+$ and $[M + \text{Li}]^+$ are similar (Figure 2), it is possible to qualitatively estimate the discrimination on Na⁺ detection by considering that below $E_{\text{Lab}} = 150$ eV, Li⁺ regeneration does not take place. The evolution profiles of the normalized TIC (Figure S6A) from the dissociation of $[M + \text{Li}]^+$ and $[M + \text{Na}]^+$ are similar when calibration used allows low mass detection. Given that the product ions related to the different three (or two) residue series are weakly less abundant for $[M + \text{Na}]^+$ at high collision energies than for $[M + \text{Li}]^+$, Na⁺ detection should not suffer from significant high-energy discrimination independently to the calibration. On the other hand, a similar comparison can be done between the normalized TIC of $[M + \text{Na}]^+$ and $[M + \text{NH}_4]^+$. In this case, using high mass calibration, the normalized TICs at the highest collision energies are also similar (Figure S6B). This contrasts with what is observed using a low-mass calibration (Figure 6A) since the normalized TIC of $[M + \text{NH}_4]^+$ becomes similar to that of $[M + \text{K}]^+$ since they show the same increase beyond $E_{\text{Lab}} = 120$ eV. At the highest energies, this reflects the formation of (i) the m/z 72 and m/z 44 product ions as the most abundant ions for $[M + \text{NH}_4]^+$ and (ii) the exclusive presence of the bare K⁺ ion from $[M + \text{K}]^+$. This is not the case of $[M + \text{Na}]^+$ and $[M + \text{Li}]^+$, which does not lead to the formation of abundant low m/z fragment ions since these immonium m/z 44 and m/z 72 species are detected in low abundances and also the Na⁺ for the $[M + \text{Na}]^+$.

Finally, comparing the rough experimental $E_{\text{Lab,Thre}}$ values of the Na⁺ and K⁺ appearance from the respective dissociation of $[M + \text{Na}]^+$ and $[M + \text{K}]^+$, with the bond energies accurately measured from the release of these alkali cations from cationized 12-crown-4-ether should suggest that they can also result from the splitting of the CS form by considering only the energy bonds.

3.2 | Selective ester cleavages of alkali-cationized cereulide species based on gas phase acidity, consequence of proton mobilization for promoting dissociation of protonated salt

The collision spectra of alkali-cationized cereulide species show, as indicated above, almost exclusively product ions with alkali retention (Figure 2; Table S2). Moreover, these cationized product ions can be classified into several series (Table S2), which are expected for peptides with non-polar side chains. First, the expected series **b** and **a** are observed. Second, the (**b** + H₂O) series are also observed (Text S3).

Surprisingly, abundant $^*\mathbf{b}_{V,(12-n)}$ and $^*\mathbf{b}_{A,(12-n)}$ product ion series, generated from the first-generation cationized fragment ions $[M + \text{K}/\text{Na}/\text{Li}-\text{C}_4\text{H}_8\text{O}]^+$ (m/z 1119, m/z 1103, and m/z 1087) (Tables S2 and Figure S4) and $[M + \text{K}/\text{Na}/\text{Li}-\text{C}_5\text{H}_{10}\text{O}]^+$ (m/z 1105 and m/z 1089 and m/z 1073) (Table S2) were observed but have not been described in previous studies.^{13,19,20} Yet they were present in the published collisional spectrum of $[M + \text{K}]^+$.^{13,19,20} The origin of $^*\mathbf{b}_{V,(12-n)}$ series is confirmed from the sequential MS³ experiments on the m/z 1119 product ion from $[M + \text{K}]^+$ (m/z 1191) (Figure S4C). Similar behavior characterizes m/z 1103 from $[M + \text{Na}]^+$ (m/z 1175) (Figure S4B) and m/z 1087 from $[M + \text{Li}]^+$ (m/z 1159) (Figure S4A) until formation of four-residue series (vide supra). MS³ spectra of $^*\mathbf{b}_{A,(12-n)}$ series are not reported.

Analysis of the main product ions of the alkali-cationized cereulide species (Table S2) is very informative because series of consecutive (or competitive) neutral losses are observed and enable efficient cereulide sequencing. They are initiated by a regioselective ring opening at the ester linkage (i.e., A-^OV or V-^OL), followed by the competitive loss of two amino acid residues (i.e., either A-^OL or V-^OV), giving rise to the **(b(o)_{V,10}** or **(b(o)_{L,10}** product ions. This is followed by stepwise consecutive losses of one residue per residue (or neutrals with a larger number of residues). However, they result in the reinforcement of both the **(b(o)_{V,(12-n)}}** or **(b(o)_{L,(12-n)}}** series with (12-n) as the even number (favored ester bond cleavages), compared to the same series with (12-n) as the odd number (amide bond cleavage). This means that ester linkage cleavage is significantly preferred to amide bond cleavage. Additionally, the same trend characterizes the derivate series (**(b(o)_{V,(12-n)-CO}**) (or **(b(o)_{L,(12-n)-CO}**), and **(b(o)_{V,(12-n) + H₂O}**) (or **(b(o)_{L,(12-n) + H₂O}**) although they are far less abundant than the **(b(o)_{V,(12-n)}}** or **(b(o)_{L,(12-n)}}** series. Finally, the $^*\mathbf{b}$ series, which were initiated by the direct initial loss of C₄H₈O (or of C₅H₁₀O), were followed only by the same neutral losses as for the **(b(o)_{V,(12-n)}}** (or **(b(o)_{L,(12-n)}}**) series. They present the same characteristics: the abundance of the product ions suddenly increased when the n values were even numbers. This orientation suggests that the C₄H₈O neutral loss (or C₅H₁₀O) is provided by the ^(O)V (or ^(O)L) residue, since the following first losses are the A and ^(O)L-A (or V and ^(O)V-V) neutral residues. On the other hand, the C₂H₄O loss is not observed as expected since the amide linkage is involved in the alanine residue. Cationized azanide is strongly unfavored, and thus, the loss of ethanimine is ruled out (vide infra).

Interestingly, the similar **b**, (**b**-CO) and (**b** + H₂O) product ion series (with a proton instead of the alkali cation) are displayed by the collisional spectrum of [M + NH₄]⁺, via the intermediate [M + H]⁺ product ion (due to ammonia loss). This behavior indicates that the bond cleavages are promoted by the charge, that is, the mobilizable proton that catalyzes the intermediate [M + H]⁺ ion dissociations. This initially occurs by an ester linkage cleavage. However, the consecutive cleavages yielding both the **b(o)**_{V,(12-n)} and **b(o)**_{L,(12-n)} series are less oriented towards that of the ester bonds. This makes a significant difference with the alkali-cationized species, although the ring opening as initial cleavage is regioselective at the ester linkage for both the ammonium and alkali adduct ions.

Like for the second-generation product ions from [M + NH₄]⁺ (via [M + H]⁺), the same cause should be associated with the CBC-related cationized product ion formation. This means that a mobilizable proton must emerge from the cationized cereulide with a structure like the PS form to promote fragmentations, whereas the alkali is spectator to the dissociations, explaining its retention in product ions. However, from small size potassiated cereulide product ions (as the four-residue product ions or smaller), the release of K⁺ is spectacularly preferred to CBC.

In order to meet such requirements, two generic PS structures could be considered:

- From intact ring alkali intermediate with alkali cation/deprotonated ester salt (i.e., ester enolate, Figure 5A) and/or alkali cation/deprotonated amide salt (Figure 5B), species having mobilized a proton either from the enolizable position of ester and/or from the NH site of amide bond. However, the observed exclusive alkali-cation retention on product ions suggests that such intermediates must be ruled out (Text S6).

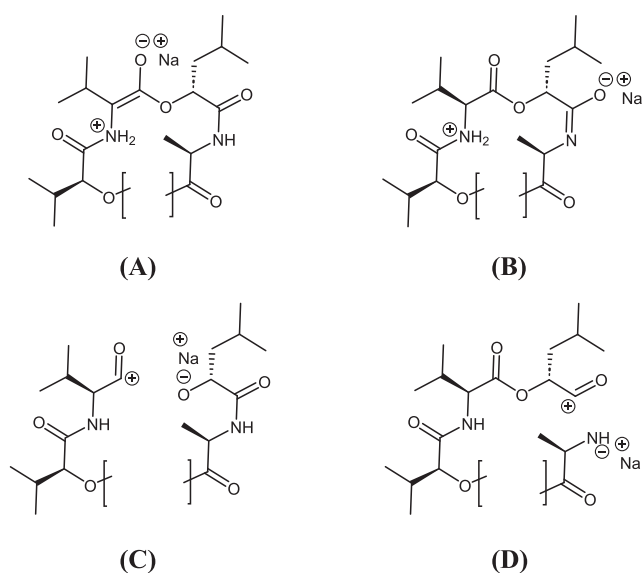


FIGURE 5 Possible salt structures of the cationized cereulide based-enolic salt with ester (A) and amide (B) groups, alkoxide (C), and azanide (D) derivate groups.

- From the opened cereulide ring intermediate with alkali cation/alkoxide salt (Figure 5C) and/or alkali cation/azanide derivate salt (Figure 5D) at one end, with a formal “acylium” group at the other end (vide infra). The latter (D) opened form with the terminus azanide salt was unfavored since the gas phase acidity of amine is very weak compared to the alcohol acidity (Table S4), and thus, this form was not considered. This description is consistent with the mechanism, herein considered as the landmark, involving both formal acylium and sodium alkoxide ends for the dissociations of sodium cyclodepsipeptide as proposed by Gross's team,⁵⁴ many years ago. Note that the C-terminus of the **b** ion series is considered as an acylium group in analytical studies to date.^{13,15,20,64,65} However, concerning the formal “acylium” terminus, a detailed mechanistic study of the formation of **b** product ion showed that the -CO-NH-CH(R)-CO⁺ terminus was much less stable than an oxazolone terminus produced by cyclization via nucleophilic CO attack on the acylium site. This oxazolone structure was first proposed by Yalcin et al.^{66–68} and then Polce et al.⁶⁹ to rationalize the **b** product ion formation. In addition, a complete study based on calculation of product ion of protonated cyclopeptides demonstrated the stability of protonated oxazolone as C-terminus of the **b**-ion series.^{70–72}

To have the interactive groups close enough to form a C-O bond giving rise concomitantly to formation of the oxazolone^{68,69,72} (i.e., the **b**' form, Figure 6), a local conformational folding of the cationized cereulide is required. The driving force behind oxazolone formation is sufficient polarization of the ester group by its proximity to the alkali cation, which induces ring opening.

Concerning the ring opening by the amide bond cleavage, a five-membered ring is formed where no mobile endocyclic

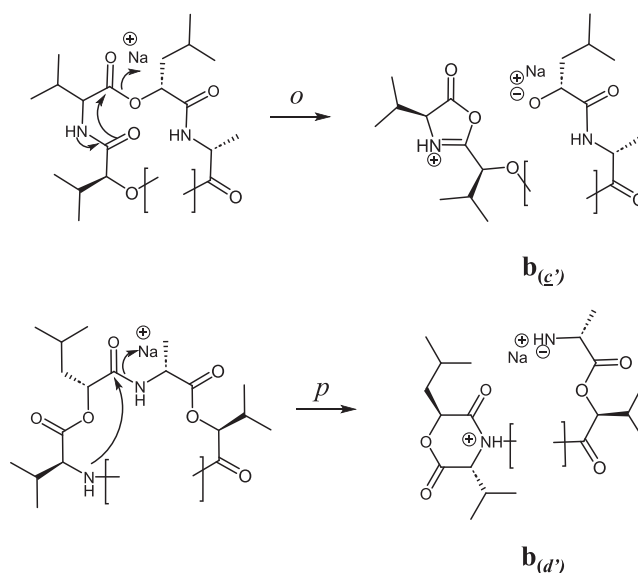
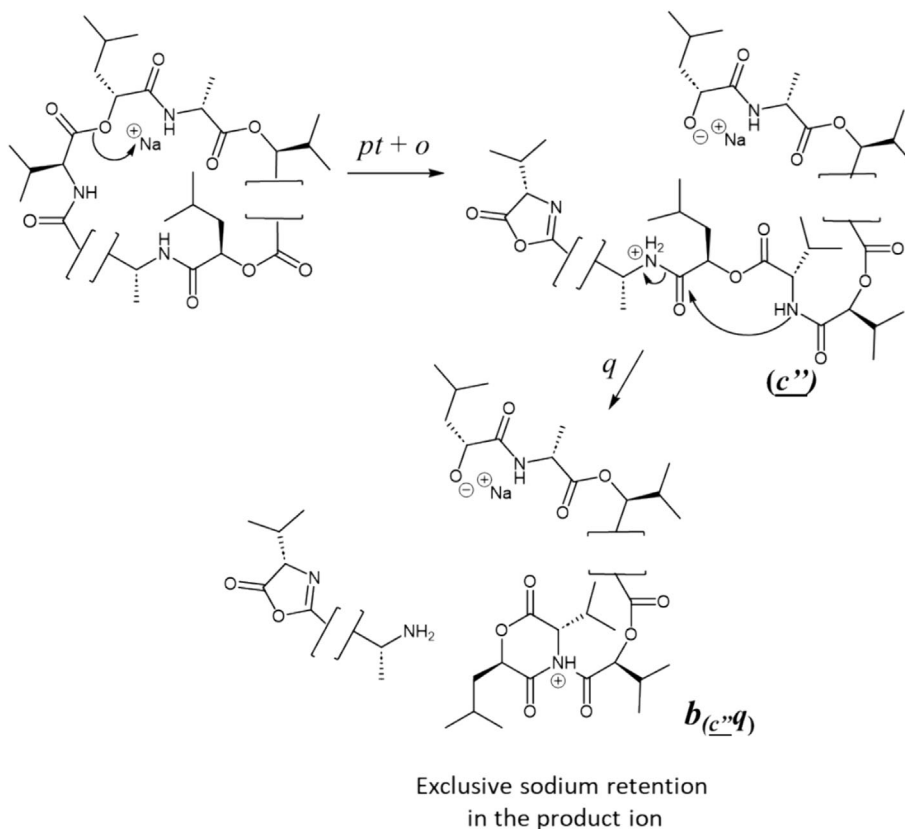


FIGURE 6 Five-membered **b**'_(o) (pathway *o*, oxazolone form) and six-membered **b**'_(p) assisting ring opening (pathway *p*, diketomorpholine form) for mobilization of proton.

FIGURE 7 Possible fragmentation mechanisms of the alkali-cationized cereulide from ring opening with the alkali-cationized alkoxide salt at one end and a terminus oxazolone c'' after migration of its proton to amide linkage inducing its cleavage into the product ion $b_{(c''q)}$.



proton (unlike protonated oxazolone) is available. Alternatively, instead of forming a five-membered ring, it could be possible to yield a six-membered ring with the NH group of the neighboring peptide bond, and thus, it results in a protonated 2,5-diketomorpholine d' (Figure 6) with a mobile endocyclic proton. As the initial amide bond cleavage is not observed, this will not be further discussed.

Alternatively, from the second form related to the alkali cation/alkoxide salt c'' (associated with the cereulide ring opening concomitantly with proton mobilization as the $[pt+o]$ pathway; Figure 7),⁷² CBC can occur via the step q , yielding the b type product ion series (i.e., the $b_{(c''q)}$ ion; Figure 7). These series exhibit exclusive alkali cation salt retention (as experimentally observed) at the backbone end with a diketomorpholine group at the other end (i.e., the $b(o)_{V,(12-n)}$ or $b(o)_{L,(12-n)}$ ion). Alkali cation retention also takes place on all other observed series.

Interestingly, the cleavages corresponding to the sodiated $b(o)_{V,(12-n)}$ or $b(o)_{L,(12-n)}$ fragment ions with $n = 6, 7, 8$ are enhanced compared to those of the potassiated cationized product ions with the same sequence. The same behavior clearly characterizes the Na^+/K^+ cationized $*b_{V,(12-n)}$ and $*b_{A,(12-n)}$ abundances with $n = 6, 7, 8$. Despite these alkali effects on product ion abundances, the collision spectra of alkali-cationized cereulide species exhibit several almost complete series of cationized fragment ions that provide unambiguous confirmation of the structure of this cyclodepsipeptide through preferential ester linkage cleavages.

4 | CONCLUSION

In electrospray, cationization of cereulide yields two general forms: *charge-solvated* (CS) and *protonated salt* (PS) forms. Their respective form depends on the alkali size, that is, with K^+ , the population of CS forms is larger than that of PS forms, and conversely with Na^+ , the CS contribution becomes negligible. This difference cannot unfortunately be attributed to ionophore cereulide selectivity towards K^+ since when the $[M + Li]^+$, $[M + Na]^+$, and $[M + K]^+$ adduct ions are desorbed from other types of compounds, very often the lithiated and sodiated molecules drive more CBC processes than the potassium ones. These alkali-cationized cereulide species dissociate by the same pathways (formation of the b , a , ($b + H_2O$), and unexpected $*b$ ion series) since the alkali cationized product ions are shifted by $+37.95 m/z$, $+21.98 m/z$, and $+6.01 m/z$ for $[M + K]^+$, $[M + Na]^+$, and $[M + Li]^+$, respectively, compared to the product ions (except the $*b$ series absent) of $[M + NH_4]^+$ (via dissociations of the $[M + H]^+$ intermediate product ion). The alkali-cationized cereulide structure is an opened cyclodepsipeptide where the ester $A-V$ and $V-L$ linkages have been selectively cleaved. This results in two opened structures with a cation/alkoxide salt at one end (and an acylium at the other). Based on this particular opened ring protonated salt, another proton migration, which takes place from the protonated oxazolone intermediate, favorably promotes the rupture at ester linkages, yielding various product ion series with alkali cation retention. In such processes, the salt end group is spectator to the dissociation, explaining why $K^+/$

Na⁺/Li⁺ promotes, through a proton mobilization, the same CBC orientation, but may influence the relative abundances of resulting cationized product ions without modifying the trends. Especially, it is shown that from the four-residue cationized product ions, alkali cations of larger size as potassium are released by splitting from PS form due to of the weakness of the ion/ion interaction force induced by the proximity of the mobile proton to the salt group. This effect was explained by using the Hard Soft Base Acid principle of Pearson based on the orbital interaction. As the contribution of the protonated salt form being major for lithiated and sodiated cereulide, their analytical use is preferable to obtain a more complete and sensitive sequence, in contrast to potassiated cereulide where the ion/ion interaction is weakened as the size of the product ions is reduced.

In order to confirm the change of the alkali-cationized cereulide conformation according to (i) the CS and PS structure and (ii) alkali size, ion mobility spectrometry (IMS) combined with MS/MS would need to be investigated. This IMS-based conformational change study would need to be addressed according to the source conditions to find out to what extent the conformation of potassiated cereulide, as it exists in solution, could be preserved in the gas phase within the *charge-solvated* form(s). Finally, the proposed alkali-cationized species interpretation will be applied to other variant sequences (called isocereulides) and other cyclodepsipeptides.

ACKNOWLEDGEMENTS

We thank Antoine Ducrocq for his technical help in using the Qq/TRAP ABSciex instrument. We also thank Craig Stevens, DESS, ELS (Coup de Puce Expansion, Toulouse, France), for English language proofreading. We are grateful to Amandine Hueber for her help in data processing of MS³ ERMS breakdown curves. We also thanks Denis Lesage for low *m/z* scattering discussion. C.C. received a grant from the French National Research Agency (Agence Nationale de la Recherche, ANR) Chiramics project (ANR-20-CE29-0017). Y.M. received a grant from the ANR Ali-mOmic project (ANR-19-CE21-0002). J.-C.T., F. F., and A.D. would like to thank the French National Infrastructure for Metabolomics and Fluxomics MetaboHUB-ANR-11-INBS-0010 and Chiramics ANR.

DATA AVAILABILITY STATEMENT

The data that support the findings of this study are available from the corresponding author upon reasonable request.

ORCID

Sophie Liuu  <https://orcid.org/0009-0009-7269-4463>

Ekaterina Darii  <https://orcid.org/0000-0001-7129-8842>

Yves Gimbert  <https://orcid.org/0000-0002-3204-4118>

François Fenaïlle  <https://orcid.org/0000-0001-6787-4149>

Gwenaëlle Lavison-Bompard  <https://orcid.org/0000-0001-6793-6290>

Olivier Firmesse  <https://orcid.org/0000-0003-2415-2802>

REFERENCES

1. SPF, Surveillance des toxi-infections alimentaires collectives (TIAC) - Données de la déclaration obligatoire, 2021. 2022.

2. EFSSA. The European Union One Health 2020 Zoonoses report. *EFSA J.* 2021;19(12):e06971.
3. They M, Cousin VL, Tissieres P, Enault M, Morin L. Multi-organ failure caused by lasagnas: a case report of *Bacillus cereus* food poisoning. *Front. Pediatr.* 2022;10:10. doi:10.3389/fped.2022.978250
4. Mahler H, Pasi A, Kramer JM, et al. Fulminant liver failure in association with the emetic toxin of *Bacillus cereus*. *N. Engl. J. Med.* 1997; 336(16):1142-1148. doi:10.1056/NEJM199704173361604
5. Takabe F, Oya M. An autopsy case of food poisoning associated with *Bacillus cereus*. *Forensic Sci.* 1976;7(2):97-101. doi:10.1016/0300-9432(76)90024-8
6. Naranjo M, Denayer S, Botteldoorn N, et al. Sudden death of a young adult associated with *Bacillus cereus* food poisoning. *J. Clin. Microbiol.* 2011;49(12):4379-4381. doi:10.1128/JCM.05129-11
7. Dirnhöfer R, Sonnabend O, Sonnabend W. Eine tödlich verlaufene Lebensmittelvergiftung durch *Bacillus cereus*. *Z. Rechtsmed.* 1977; 80(2):139-151. doi:10.1007/BF01160201
8. Shiota M, Saitou K, Mizumoto H, et al. Rapid detoxification of cereulide in *Bacillus cereus* food poisoning. *Pediatrics.* 2010;125(4):e951-e955. doi:10.1542/peds.2009-2319
9. Dierick K, Coillie EV, Swiecicka I, et al. Fatal family outbreak of *Bacillus cereus*-associated food poisoning. *J. Clin. Microbiol.* 2005;43(8): 4277-4279. doi:10.1128/JCM.43.8.4277-4279.2005
10. Yang S, Wang Y, Liu Y, Jia K, Zhang Z, Dong Q. Cereulide and emetic *Bacillus cereus*: characterizations, impacts and public precautions. *Foods.* 2023;12(4):833. doi:10.3390/foods12040833
11. Suwan S, Isobe M, Ohtani I, Agata N, Mori M, Ohta M. Structure of cereulide, a cyclic dodecadepsipeptide toxin from *Bacillus cereus* and studies on NMR characteristics of its alkali metal complexes including a conformational structure of the K⁺ complex. *J. Chem. Soc. Perkin. Trans.* 1995;1(7):765-775.
12. García-Calvo J, Ibeas S, Antón-García E-C, et al. Potassium-ion-selective fluorescent sensors to detect Cereulide, the emetic toxin of *B. cereus*, in food samples and HeLa cells. *ChemistryOpen.* 2017;6(4): 562-570. doi:10.1002/open.201700057
13. Marxen S, Stark TD, Frenzel E, et al. Chemodiversity of cereulide, the emetic toxin of *Bacillus cereus*. *Anal. Bioanal. Chem.* 2015;407(9): 2439-2453. doi:10.1007/s00216-015-8511-y
14. Mikkola R, Saris N-EL, Grigoriev PA, Andersson MA, Salkinoja-Salonen MS. Ionophoretic properties and mitochondrial effects of cereulide. *Eur. J. Biochem.* 1999;263(1):112-117. doi:10.1046/j.1432-1327.1999.00476.x
15. Ducrest PJ, Pfammatter S, Stephan D, Vogel G, Thibault P, Schnyder B. Rapid detection of *Bacillus* ionophore cereulide in food products. *Sci. Rep.* 2019;9(1):5814. doi:10.1038/s41598-019-42167-0
16. Cavellier F, Enjalbal C, Martinez J, Roque M, Sanchez P, Aubagnac J-L. Comparison of collisionally activated dissociation mass spectra for the identification of cyclopeptides and cyclodepsipeptides. *Rapid Commun. Mass Spectrom.* 1999;13(10):880-885. doi:10.1002/(SICI)1097-0231(19990530)13:10<880::CO:2-1
17. Pitchayawasin S, Kuse M, Koga K, Isobe M, Agata N, Ohta M. Complexation of cyclic dodecadepsipeptide, Cereulide with ammonium salts. *Bioorg. Med. Chem. Lett.* 2003;13(20):3507-3512. doi:10.1016/S0960-894X(03)00731-5
18. In't Veld PH, van der Laak LFJ, van Zon M, Biesta-Peters EG. Elaboration and validation of the method for the quantification of the emetic toxin of *Bacillus cereus* as described in EN-ISO 18465—microbiology of the food chain—quantitative determination of emetic toxin (cereulide) using LC-MS/MS. *Int. J. Food Microbiol.* 2019;288:91-96. doi:10.1016/j.ijfoodmicro.2018.03.021
19. Walser V, Kranzler M, Ehling-Schulz M, Stark TD, Hofmann TF. Structure revision of Isocereulide A, an isoform of the food poisoning emetic *Bacillus cereus* toxin cereulide. *Molecules.* 2021;26(5):1360. doi:10.3390/molecules26051360

20. Walser V, Kranzler M, Dawid C, Ehling-Schulz M, Stark TD, Hofmann TF. *Bacillus cereus* toxin repertoire: diversity of (Iso)cereulide(s). *Molecules*. 2022;27(3):872. doi:10.3390/molecules27030872
21. Armentrout PB. Energetics and mechanisms for decomposition of cationized amino acids and peptides explored using guided ion beam tandem mass spectrometry. *Mass Spectrom. Rev.* 2023;42(3):928-953. doi:10.1002/mas.21723
22. Wyttenbach T, Witt M, Bowers MT. On the question of salt bridges of cationized amino acids in the gas phase: glycine and arginine. Dedicated to the memory of Ben Freiser. *Int. J. Mass. Spectrom.* 1999; 182-183:243-252. doi:10.1016/S1387-3806(98)14255-0
23. Strittmatter EF, Williams ER. The role of proton affinity, acidity, and electrostatics on the stability of neutral versus ion-pair forms of molecular dimers. *Int. J. Mass. Spectrom.* 2001;212(1):287-300. doi:10.1016/S1387-3806(01)00475-4
24. Colsch B, Fenaille F, Warnet A, Junot C, Tabet J-C. Mechanisms governing the fragmentation of glycerophospholipids containing choline and ethanolamine polar head groups. *Eur. J. Mass. Spectrom.* 2017; 23(6):427-444. doi:10.1177/1469066717731668
25. Colsch B, Damont A, Junot C, Fenaille F, Tabet J-C. Experimental evidence that electrospray-produced sodiated lysophosphatidyl ester structures exist essentially as protonated salts. *Eur. J. Mass. Spectrom.* 2019;25(3):333-338. doi:10.1177/1469066719838924
26. Damont A, Olivier M-F, Warnet A, et al. Proposal for a chemically consistent way to annotate ions arising from the analysis of reference compounds under ESI conditions: a prerequisite to proper mass spectral database constitution in metabolomics. *J. Mass Spectrom.* 2019; 54(6):567-582. doi:10.1002/jms.4372
27. Lee S-W, Kim HS, Beauchamp JL. Salt bridge chemistry applied to gas-phase peptide sequencing: selective fragmentation of sodiated gas-phase peptide ions adjacent to aspartic acid residues. *J. Am. Chem. Soc.* 1998;120(13):3188-3195. doi:10.1021/ja973467r
28. Lemoff AS, Bush MF, Williams ER. Binding energies of water to sodiated valine and structural isomers in the gas phase: the effect of proton affinity on zwitterion stability. *J. Am. Chem. Soc.* 2003; 125(44):13576-13584. doi:10.1021/ja034544n
29. Lemoff AS, Bush MF, Williams ER. Structures of cationized proline analogues: evidence for the zwitterionic form. *Chem. A Eur. J.* 2005; 109(9):1903-1910. doi:10.1021/jp0466800
30. Kapota C, Lemaire J, Maître P, Ohanessian G. Vibrational signature of charge solvation vs salt bridge isomers of sodiated amino acids in the gas phase. *J. Am. Chem. Soc.* 2004;126(6):1836-1842. doi:10.1021/ja036932v
31. Kapota C, Ohanessian G. The low energy tautomers and conformers of the dipeptides HisGly and GlyHis and of their sodium ion complexes in the gas phase. *Phys. Chem. Chem. Phys.* 2005;7(21):3744-3755. doi:10.1039/b508092d
32. Heiles S, Berden G, Oomens J, Williams ER. Competition between salt bridge and non-zwitterionic structures in deprotonated amino acid dimers. *Phys. Chem. Chem. Phys.* 2018;20(23):15641-15652. doi:10.1039/C8CP01458B
33. Kish MM, Wesdemiotis C. Selective cleavage at internal lysine residues in protonated vs. metalated peptides. *Int. J. Mass. Spectrom.* 2003;227(1):191-203. doi:10.1016/S1387-3806(03)00069-1
34. Balaj OP, Kapota C, Lemaire J, Ohanessian G. Vibrational signatures of sodiated oligopeptides (GG-Na⁺, GGG-Na⁺, AA-Na⁺ and AAA-Na⁺) in the gas phase. *Int. J. Mass. Spectrom.* 2008;269(3):196-209. doi:10.1016/j.ijms.2007.10.004
35. Darii E, Alves S, Gimbert Y, Perret A, Tabet J-C. Meaning and consequence of the coexistence of competitive hydrogen bond/salt forms on the dissociation orientation of non-covalent complexes. *J. Chromatogr. B.* 2017;1047:45-58. doi:10.1016/j.jchromb.2016.09.038
36. Darii E, Gimbert Y, Alves S, et al. First direct evidence of Interpartner hydride/deuteride exchanges for stored sodiated arginine/fructose-6-phosphate complex anions within salt-solvated structures. *J. Am. Soc. Mass Spectrom.* 2021;32(6):1424-1440. doi:10.1021/jasms.1c00040
37. Tabet J-C, Gimbert Y, Damont A, Touboul D, Fenaille F, Woods AS. Combining chemical knowledge and quantum calculation for interpreting low-energy product ion spectra of metabolite adduct ions: sodiated diterpene diester species as a case study. *J. Am. Soc. Mass Spectrom.* 2021;32(10):2499-2504. doi:10.1021/jasms.1c00154
38. Crevelin EJ, Crotti AEM, Zucchi TD, Melo IS, Moraes LAB. Dereplication of streptomycetes sp. AMC 23 polyether ionophore antibiotics by accurate-mass electrospray tandem mass spectrometry. *J. Mass Spectrom.* 2014;49(11):1117-1126. doi:10.1002/jms.3432
39. Demarque DP, Crotti AEM, Vessecchi R, Lopes JLC, Lopes NP. Fragmentation reactions using electrospray ionization mass spectrometry: an important tool for the structural elucidation and characterization of synthetic and natural products. *Nat. Prod. Rep.* 2016;33(3):432-455. doi:10.1039/C5NP00073D
40. Decler M, Rajkovic A, Sas B, Madder A, de Saeger S. Development and validation of ultra-high-performance liquid chromatography-tandem mass spectrometry methods for the simultaneous determination of beauvericin, enniatins (A, A1, B, B1) and cereulide in maize, wheat, pasta and rice. *J. Chromatogr. A.* 2016;1472:35-43. doi:10.1016/j.chroma.2016.10.003
41. Cooks RG, Beynon JH. Metastable ions and ion kinetic energy spectrometry: the development of a new research area. *J. Chem. Educ.* 1974;51(7):437. doi:10.1021/ed051p437
42. Bennaceur C, Afonso C, Alves S, Bossée A, Tabet J-C. Instrumental dependent dissociations of n-propyl/isopropyl phosphonate isomers: evaluation of resonant and non-resonant vibrational activations. *J. Am. Soc. Mass Spectrom.* 2013;24(8):1260-1270. doi:10.1007/s13361-013-0656-3
43. Schwarzenberg A, Dossman H, Cole RB, Machuron-Mandard X, Tabet J-C. Differentiation of isomeric dinitrotoluenes and aminodinitrotoluenes using electrospray high resolution mass spectrometry. *J. Mass Spectrom.* 2014;49(12):1330-1337. doi:10.1002/jms.3471
44. Fedor DM, Cooks RG. Angle resolved mass spectrometry with a reversed geometry spectrometer. *Anal. Chem.* 1980;52(4):679-682. doi:10.1021/ac50054a021
45. Bourehil L, Soep C, Seng S, et al. Bond-dissociation energies to probe pyridine electronic effects on organogold (III) complexes: from methodological developments to application in π -backdonation investigation and catalysis. *Inorg. Chem.* 2023;62(33):13304-13314. doi:10.1021/acs.inorgchem.3c01584
46. Hueber A, Green M, Ujma J, et al. Energy-resolved ion mobility spectrometry: composite breakdown curves for distinguishing isomeric product ions. *J. Am. Soc. Mass Spectrom.* 2023;34(1):36-47. doi:10.1021/jasms.2c00233
47. Hueber A, Kulyk H, Damont A, et al. Energy resolved mass spectrometry for interoperable non-resonant collisional spectra in metabolomics. *J. Am. Soc. Mass Spectrom.* 2024;35(5):834-838. doi:10.1021/jasms.3c00410
48. Murray KK, Boyd RK, Eberlin MN, Langley GJ, Li L, Naito Y. Definitions of terms relating to mass spectrometry (IUPAC recommendations 2013). *Pure Appl. Chem.* 2013;85(7):1515-1609. doi:10.1351/PAC-REC-06-04-06
49. Olsen JV, Macek B, Lange O, Makarov A, Horning S, Mann M. Higher-energy C-trap dissociation for peptide modification analysis. *Nat. Methods.* 2007;4(9):709-712. doi:10.1038/nmeth1060
50. Lopez LL, Tiller PR, Senko MW, Schwartz JC. Automated strategies for obtaining standardized collisionally induced dissociation spectra on a benchtop ion trap mass spectrometer. *Rapid Commun. Mass Spectrom.* 1999;13(8):663-668. doi:10.1002/(SICI)1097-0231(19990430)13:8<663::CO:2-H
51. Xue B, Alves S, Desbans C, et al. Heparin-like glycosaminoglycan/amine salt-bridge interactions: a new potential

- tool for HLGAGs analysis using mass spectrometry. *J. Mass Spectrom.* 2011;46(7):689-695. doi:[10.1002/jms.1939](https://doi.org/10.1002/jms.1939)
52. DeMuth JC, McLuckey SA. Electrospray droplet exposure to organic vapors: metal ion removal from proteins and protein complexes. *Anal. Chem.* 2015;87(2):1210-1218. doi:[10.1021/ac503865v](https://doi.org/10.1021/ac503865v)
 53. Rush MD, van Breemen RB. Role of ammonium in the ionization of phosphatidylcholines during electrospray mass spectrometry. *Rapid Commun. Mass Spectrom. RCM.* 2017;31(3):264-268. doi:[10.1002/rcm.7788](https://doi.org/10.1002/rcm.7788)
 54. Ngoka LCM, Gross ML, Toogood PL. Sodium-directed selective cleavage of lactones: a method for structure determination of cyclodepsipeptides. Dedicated to the memory of Professor Ben S. Freiser. *Int. J. Mass Spectrom.* 1999;182-183:289-298. doi:[10.1016/S1387-3806\(98\)14248-3](https://doi.org/10.1016/S1387-3806(98)14248-3)
 55. Li Y, He N, Luo M, Hong B, Xie Y. Application of untargeted tandem mass spectrometry with molecular networking for detection of enniatins and beauvericins from complex samples. *J. Chromatogr. A.* 2020; 1634:461626. doi:[10.1016/j.chroma.2020.461626](https://doi.org/10.1016/j.chroma.2020.461626)
 56. Uhlig S, Ivanova L, Petersen D, Kristensen R. Structural studies on minor enniatins from *Fusarium* sp. VI 03441: novel N-methyl-threonine containing enniatins. *Toxicon.* 2009;53(7):734-742. doi:[10.1016/j.toxicon.2009.02.014](https://doi.org/10.1016/j.toxicon.2009.02.014)
 57. Williams SM, Brodbelt JS. MSn characterization of protonated cyclic peptides and metal complexes. *J. Am. Soc. Mass Spectrom.* 2004;15(7): 1039-1054. doi:[10.1016/j.jasms.2004.03.015](https://doi.org/10.1016/j.jasms.2004.03.015)
 58. Brandon EFA, van Ooijen RD, Sparidans RW, et al. Structure elucidation of aplidine metabolites formed in vitro by human liver microsomes using triple quadrupole mass spectrometry. *J. Mass Spectrom.* 2005;40(6):821-831. doi:[10.1002/jms.863](https://doi.org/10.1002/jms.863)
 59. Taibon J, Sturm S, Seger C, Parth M, Strasser H, Stuppner H. Development of a fast and selective UHPLC-DAD-QTOF-MS/MS method for the qualitative and quantitative assessment of destruxin profiles. *Anal. Bioanal. Chem.* 2014;406(29):7623-7632. doi:[10.1007/s00216-014-8203-z](https://doi.org/10.1007/s00216-014-8203-z)
 60. Banerjee R, Sudaralal S, Ranganayaki RS, Raghothama S. Effect of ester chemical structure and peptide bond conformation in fragmentation pathways of differently metal cationized cyclodepsipeptides. *Org. Biomol. Chem.* 2011;9(18):6234-6245. doi:[10.1039/c1ob05392b](https://doi.org/10.1039/c1ob05392b)
 61. Pearson RG. Hard and soft acids and bases. *J. Am. Chem. Soc.* 1963; 85(22):3533-3539. doi:[10.1021/ja00905a001](https://doi.org/10.1021/ja00905a001)
 62. Pearson RG. Chemical hardness and density functional theory. *J. Chem. Sci.* 2005;117(5):369-377. doi:[10.1007/BF02708340](https://doi.org/10.1007/BF02708340)
 63. Armentrout PB. Cation-ether complexes in the gas phase: thermodynamic insight into molecular recognition. *Int. J. Mass Spectrom.* 1999; 193(2):227-240. doi:[10.1016/S1387-3806\(99\)00165-7](https://doi.org/10.1016/S1387-3806(99)00165-7)
 64. Pitchayawasin S, Isobe M, Kuse M, Franz T, Agata N, Ohta M. Molecular diversity of cereulide detected by means of nano-HPLC-ESI-Q-TOF-MS. *Int. J. Mass Spectrom.* 2004;235(2):123-129. doi:[10.1016/j.ijms.2004.04.007](https://doi.org/10.1016/j.ijms.2004.04.007)
 65. Bauer T, Stark T, Hofmann T, Ehling-Schulz M. Development of a stable isotope dilution analysis for the quantification of the *Bacillus cereus* toxin cereulide in foods. *J. Agric. Food Chem.* 2010;58(3):1420-1428. doi:[10.1021/jf9033046](https://doi.org/10.1021/jf9033046)
 66. Yalcin T, Khouw C, Csizmadia IG, Peterson MR, Harrison AG. Why are B ions stable species in peptide spectra? *J. Am. Soc. Mass Spectrom.* 1995;6(12):1165-1174. doi:[10.1016/1044-0305\(95\)00569-2](https://doi.org/10.1016/1044-0305(95)00569-2)
 67. Yalcin T, Csizmadia IG, Peterson MR, Harrison AG. The structure and fragmentation of Bn ($n \geq 3$) ions in peptide spectra. *J. Am. Soc. Mass Spectrom.* 1996;7(3):233-242. doi:[10.1016/1044-0305\(95\)00677-X](https://doi.org/10.1016/1044-0305(95)00677-X)
 68. Yalcin T, Harrison AG. Ion chemistry of protonated lysine derivatives. *J. Mass Spectrom.* 1996;31(11):1237-1243. doi:[10.1002/\(SICI\)1096-9888\(199611\)31:113.0.CO;2-P](https://doi.org/10.1002/(SICI)1096-9888(199611)31:113.0.CO;2-P)
 69. Polce MJ, Ren D, Westemiotis C. Dissociation of the peptide bond in protonated peptides. *J. Mass Spectrom.* 2000;35(12):1391-1398. doi:[10.1002/1096-9888\(200012\)35:123.0.CO;2-1](https://doi.org/10.1002/1096-9888(200012)35:123.0.CO;2-1)
 70. Paizs B, Suhai S. Towards understanding the tandem mass spectra of protonated oligopeptides. 1: mechanism of amide bond cleavage. *J. Am. Soc. Mass Spectrom.* 2004;15(1):103-113. doi:[10.1016/j.jasms.2003.09.010](https://doi.org/10.1016/j.jasms.2003.09.010)
 71. Jegorov A, Paizs B, Kuzma M, et al. Extraribosomal cyclic tetradepsipeptides beauverolides: profiling and modeling the fragmentation pathways. *J. Mass Spectrom.* 2004;39(8):949-960. doi:[10.1002/jms.674](https://doi.org/10.1002/jms.674)
 72. Paizs B, Suhai S. Fragmentation pathways of protonated peptides. *Mass Spectrom. Rev.* 2005;24(4):508-548. doi:[10.1002/mas.20024](https://doi.org/10.1002/mas.20024)

SUPPORTING INFORMATION

Additional supporting information can be found online in the Supporting Information section at the end of this article.

How to cite this article: Liuu S, Trinh Ke, Darii E, et al. Charge-solvated versus protonated salt forms of cyclodepsipeptide toxins in electrospray: Dissociation of alkali-cationized forms enables straightforward sequencing of cereulide. *J Mass Spectrom.* 2024;59(6):e5037. doi:[10.1002/jms.5037](https://doi.org/10.1002/jms.5037)